

CrystEngComm

Accepted Manuscript



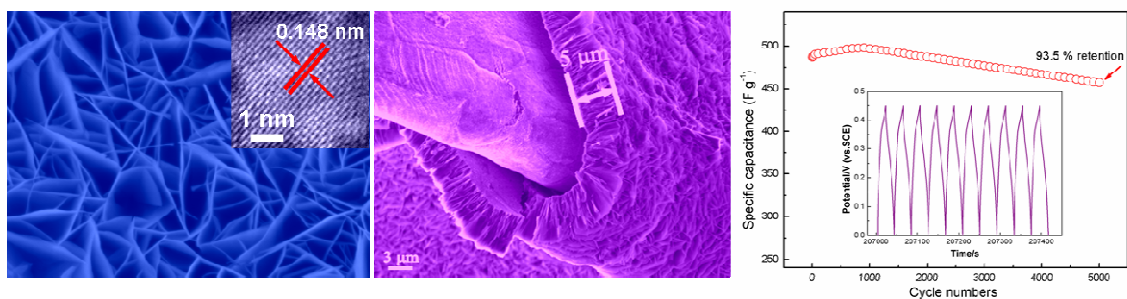
This is an *Accepted Manuscript*, which has been through the Royal Society of Chemistry peer review process and has been accepted for publication.

Accepted Manuscripts are published online shortly after acceptance, before technical editing, formatting and proof reading. Using this free service, authors can make their results available to the community, in citable form, before we publish the edited article. We will replace this *Accepted Manuscript* with the edited and formatted *Advance Article* as soon as it is available.

You can find more information about *Accepted Manuscripts* in the [Information for Authors](#).

Please note that technical editing may introduce minor changes to the text and/or graphics, which may alter content. The journal's standard [Terms & Conditions](#) and the [Ethical guidelines](#) still apply. In no event shall the Royal Society of Chemistry be held responsible for any errors or omissions in this *Accepted Manuscript* or any consequences arising from the use of any information it contains.

Graphical abstract



The single-crystalline NiO nanosheet arrays on Ni foam with a thickness about 5 μm as a binder-free electrode for high-performance supercapacitor were fabricated by a facile and cost-effective hydrothermal approach.

The unique designed NiO nanosheet arrays on Ni foam have exhibited a high specific capacitance (674.2 F g⁻¹ at a current density of 1 A g⁻¹), good rate capability, and excellent cycling stability (93.5% capacitance retention after 5000 cycles).

Facile synthesis of single-crystalline NiO nanosheet arrays on Ni foam for high-performance supercapacitors

Ming Huang^a, Fei Li^a, Junyi Ji^{b,*}, Yu Xin Zhang^{a,c,*}, Xiao Li Zhao^a, Xing Gao^a

Abstract

Mesoporous NiO single-crystalline nanosheet arrays grown on Ni foam with a thickness about 5 μm have been fabricated by a facile hydrothermal approach and further investigated as the binder-free electrode for high-performance supercapacitors. Owing to the high conductivity of the single-crystalline NiO nanosheet arrays on conducting substrate in combination with the large surface area provided by the mesoporous NiO nanosheets, the unique designed NiO nanosheet arrays on Ni foam have exhibited a high specific capacitance (674.2 F g^{-1} at a current density of 1 A g^{-1}), good rate capability, and excellent cycling stability (93.5% capacitance retention after 5000 cycles). These results suggest that the single-crystalline NiO nanosheet arrays electrode is a promising candidate for high-performance supercapacitor and the rational design of the unique binder-free electrode demonstrated in this work provides a new and facile approach to fabricate other transition metal oxides arrays for electrochemical energy storage.

Keywords: Nickel oxide; Single-crystalline; Binder-free; Nanosheet arrays; Supercapacitors

1. Introduction

With the ever-increasing power and energy demand in modern consumer electronic devices and electric vehicles, the development of high-performance, lightweight and environmental friendly energy storage devices has attracted tremendous attention.¹⁻⁴ Among various emerging energy storage technologies, supercapacitors with irreplaceable properties of high power density, fast charge-discharge rate, and stable cycling performance, have become promising candidates in the energy storage areas.⁵⁻⁷ Based on

the charge storage mechanisms, they can be divided into two categories, namely, electric double layer capacitors (EDLCs) and pseudocapacitors.⁸ Pseudocapacitor, in which charge is stored using redox-based Faradic reactions, can have higher capacitances than EDLCs. In particular, transition metal oxides with variable valence are considered as ideal electrodes materials for pseudocapacitors as they can provide a variety of oxidation states for efficient redox charge transfer.⁹⁻¹² To date, it is well established that RuO₂ is a prominent electroactive material for supercapacitors due to the high specific capacitance and excellent reversibility.^{13,14} However, it is not widely used owing to the high cost, rare resources, and environmental toxicity. Therefore, great efforts have been devoted to searching for inexpensive and environmentally friendly transition metal oxides with good capacitive characteristics, such as Co₃O₄,¹⁵ NiO,¹⁶ MnO₂,¹⁷ CuO,¹⁸ and V₂O₅.¹⁹

Among these candidate materials, NiO exhibits many intriguing characteristics, such as low cost, environmental friendliness, natural abundance, and high theoretical capacity (2573 F g⁻¹), suggesting it as the most promising electrode material for supercapacitors. Until now, different NiO nanostructures, including porous spheres,²⁰ nanoflowers,²¹ nanoflakes,²² nanotubes,²³ and nanobelts,²⁴ have been investigated as electrodes in supercapacitors. However, the low surface area and poor electrical conductivity of NiO limits the ion and electron transfer rate for high-performance supercapacitors. Moreover, the conventional strategies for the fabrication of NiO electrodes are related to mixing and pressing powder of active material with ancillary materials such as carbon black or binder would lead to a compact structure which is unfavorable for fast electron transfer and electrolyte diffusion, hindering their high electrochemical performance. An emerging attractive concept is to directly grow NiO arrays with mesoporous structures on conducting substrates as free-standing and binder-free electrodes for supercapacitors which can not only avoid the tedious electrode preparation process but

also enhance the conductivity and effective utilization of the active materials as every electroactive nanostructure is directly attached to the conductive substrate, resulting in high capacitance, long cycle life, and high rate capability.²⁵⁻³¹ Thus, a novel but simple design and fabrication of a stable NiO electrode with highly-accessible surface areas and fast ion diffusion for high-performance supercapacitor based on this cost-effective strategy still remains a challenge.

In this work, we demonstrate a facile and cost-effective approach to design and fabricate single-crystalline NiO nanosheet arrays on Ni foam as a binder-free electrode for high-performance supercapacitors. Benefiting from the favorable mesoporous NiO nanosheets as well as the rational design of binder-free electrode, the NiO nanosheet arrays on Ni foam electrode exhibits a much higher capacitance (674.2 F g^{-1} at a current density of 1 A g^{-1}) and excellent cycling ability (93.5% retention after 5000 cycles). Undoubtedly, the facile design of binder-free NiO nanosheet arrays electrode demonstrated in this work offers a promising strategy for the fabrication of high-performance electrodes for supercapacitors.

2. Experimental

2.1 Synthesis of NiO nanosheet arrays on Ni foam

All the chemical reagents were of analytical purity and used without any further purification. NiO nanosheet arrays on Ni foam were synthesized by a simple hydrothermal method. In a typical procedure, $\text{Ni}(\text{NO}_3)_2 \cdot 6\text{H}_2\text{O}$ (0.582 g, 2 mmol), NH_4F (0.148 g, 4 mmol) and $\text{CO}(\text{NH}_2)_2$ (0.601 g, 10 mmol) were dissolved in 50 mL deionized water and vigorously stirred for 10 min to obtain a transparent solution. Nickel foam ($1 \times 3 \text{ cm}^2$) was carefully cleaned with 3 M HCl solution in an ultrasound bath for 5 min to remove the surface NiO layer, and then cleaned with deionized water and ethanol for 5 min each. The aqueous solution and the Ni foam were transferred to a Teflon-lined

stainless-steel autoclave and maintained at 105 °C for 5 h, and then cooled down to room temperature. The samples were rinsed several times with deionized water and ethanol with the assistance of ultrasonication, and dried at 80 °C for 8 h. Finally, the sample was annealed in air at 350 °C for 2 h to obtain mesoporous NiO nanosheet arrays on Ni foam. The loading density of the NiO on Ni foam is calculated to be 2.52 mg/cm².

2.2 Materials characterization

The crystallographic information and chemical composition of as-prepared products were established by powder X-ray diffraction (XRD, D/max 1200, Cu K α). The thermal behavior of Ni foam was investigated by the thermogravimetric analyzer-differential scanning calorimeter (TGA-DSC, NETZSCH STA 449C). The morphological investigations were carried out with focused ion beam (Zeiss Auriga FIB/SEM). The elemental composition was evaluated using the electron microscope TESCAN VEGA to fully experience the EDS analysis. Microstructures were characterized by high-resolution transmission electron microscopy (HRTEM, Zeiss Libra 200). Nitrogen adsorption-desorption isotherms were measured at 77 K with micrometric ASAP 2020 sorptometer. The specific surface area was calculated with the Brunauer-Emmett-Teller (BET) equation, and the pore size distribution was calculated from the adsorption curve by the Barrett-Joyner-Halenda (BJH) method.

2.3 Electrochemical measurements

The electrochemical tests were performed on the CHI 660E electrochemical workstation at room temperature in a three-electrode configuration. The mesoporous NiO nanosheet arrays on Ni foam (1 × 1.5 cm²) was directly used as the working electrode. A platinum plate and a saturated calomel electrode (SCE) were served as the counter electrode and reference electrode, respectively. Freshly prepared

KOH (1 M) aqueous solution was used as the electrolyte. The cyclic voltammetry (CV) and galvanostatic charging/discharging techniques were employed to investigate the electrochemical performance of the NiO electrode. The electrochemical impedance spectroscopy (EIS) was conducted in the frequency range between 100 kHz and 0.01 Hz with a perturbation amplitude of 5 mV versus the open-circuit potential.

3. Results and discussion

3.1 Structure and morphology

The XRD pattern of the as-prepared NiO nanosheets arrays on Ni foam is shown in Fig. 1. Excluding the strong peaks originating from the Ni foam, the diffraction peaks of NiO nanosheet arrays are observed of 37.3 °, 43.3 °, and 62.9 °, which could be assigned to the (110), (200), and (220) planes of the cubic NiO, respectively, which is in accord with the standard XRD pattern of bunsenite NiO (JCPDS card no. 47-1049). No signal from other crystalline phases could be detected, indicating the high purity of the obtained NiO nanosheets.

The morphologies of Ni foam and the mesoporous NiO nanosheet arrays on Ni foam are investigated by scanning electron microscopy (SEM). Fig. 2a shows a representative low-magnification SEM image of the pristine Ni foam with smooth surface before NiO nanosheets growth. Moreover, the typical SEM image and the corresponding EDS mapping of the Ni foam after annealing in air were investigated (see **Electronic Supplementary Information (ESI), Fig. S1**). There was no notable oxide layer detected, indicating that is stable to a certain extent in air until 350 °C, which is consistent with the thermal gravity analysis curve of the bare Ni foam (see **ESI, Fig. S2**). After NiO nanosheets growth, the surface of the Ni foam becomes rough as revealed in Fig. 2b, indicating the growth of NiO nanosheets over a large area. The inset in Fig. 2a and b displays the optical images of the pristine Ni

foam and NiO nanosheet arrays on Ni foam. The surface color of the Ni foam changed from silver-white to black also demonstrates the NiO growth. Fig. 2c and d show the enlarged SEM images of the NiO nanosheet arrays grown on Ni foam. Obviously, the NiO nanosheets are homogeneously aligned and separated apart adequately, forming a unique nanoarray with a highly open and porous structure on a large scale, which endows the fast transport of electrolyte. These NiO nanosheets have an edge length of 1-3 μm and a uniform thickness of less than 50 nm. The cross-section image (see ESI, Fig. S3) reveals the thickness of the prepared NiO nanosheet arrays is around 5 μm , indicating a large loading mass of the active material. The EDS data of the NiO nanosheet arrays on Ni foam was also investigated (see ESI, Fig. S4). Furthermore, the adhesion of the NiO nanosheet arrays on the Ni foam skeleton is compact and strong, considering the fact that the sample sustains a long ultrasonication for about 30 minutes before the SEM measurements.

The microstructures of the mesoporous NiO nanosheet were further investigated by TEM (Fig. 3). Fig. 3a and b show the low-magnification TEM images of a single NiO nanosheet. The nanosheet is composed of numerous cross-linked nanoparticles with diameters of 5-20 nm, and shows a mesoporous structure with a pore size of 2-5 nm. Accordingly, the electrolyte can be easily soaked into these porosity structure while the thin nanosheet morphology (<50 nm thickness) reduces the diffusion length of OH^- in the active material (NiO nanosheets), thus maximizes the active surface area for insertion and extrusion of OH^- , which would enable the achievement of high rate capability.^{27, 32} The SAED pattern in the inset of Fig. 3b has confirmed the nature of a single crystal. It can be indexed as the cubic structure without any detectable secondary phase. Furthermore, the SAED pattern presented a hexagonal alignment of {220} spots, which corresponded to the diffraction pattern along the [111] zone axis of the NiO crystal.^{25, 33, 34} The HRTEM image (Fig. 3c) shows the lattice fringes with a spacing

distance of 0.148 nm, corresponding to the (220) planes of face-centered cubic NiO, which agreed well with the XRD result and SAED pattern.^{35, 36}

3.2 Surface area and porosity analysis

To more clearly describe the porous features, the N₂ adsorption-desorption measurements were performed to study the porosity and textural properties of the mesoporous NiO nanosheets. Fig. 4 depicts the adsorption-desorption isotherm and pore size distribution for the NiO nanosheets scratched down from the Ni foam. The isotherm can be classified as type IV according to the profile of a hysteresis loop in a relative pressure (P/P₀) range of 0.5-1.0. This reveals that the as-prepared NiO nanosheet has a typical mesoporous structure, which is further verified from the Barrett-Joyner-Halenda (BJH) pore size distribution (PSD) data shown in Fig. 4b. Nitrogen adsorption-desorption results indicate that the mesoporous NiO nanosheets has a BET surface area of 111.6 m² g⁻¹ with a pore volume of 0.13 cm³ g⁻¹. The pore size distribution obtained from the adsorption branch by the Barrett-Joyner-Halenda (BJH) method indicates that the average pore size is ~4.3 nm. Such unique mesoporous NiO nanosheet arrays with high specific surface area own numerous open channels, as shown in Fig. 2c and d, which facilitates the fast diffusion of electrolyte ions to the NiO nanosheets for efficient energy storage, ensuring the high electrochemical capacity for the NiO nanosheet arrays.

3.3 Electrochemical properties

In order to evaluate the electrochemical characteristics of the free-standing mesoporous NiO nanosheet arrays, the NiO nanosheet arrays on Ni foam have been directly used as working electrode to characterize its electrochemical properties in a three-electrode configuration. Fig. 5a shows the CV curves of the NiO nanosheet arrays in 1 M KOH electrolyte at various scan rates ranged from 2 to 50

mV s⁻¹ in the potential window of 0 to 0.45 V (*vs.* SCE). Although there are no distinct redox peaks at high scan rate (50 mV s⁻¹), the shape of the CV curves deviate from the ideal rectangle, indicating the Faradic pseudocapacitive nature of the NiO electrode, which can be proved by the CV curves measured at lower scan rates (see ESI, Fig. S5). Moreover, as the scan rate increases, the current subsequently increases while the CV shape changes little, which demonstrates the fast electrons and ions diffusion rate in the NiO electrode.

To further examine the electrochemical performances of the NiO nanosheet arrays electrode, we perform galvanostatic constant current charge-discharge curves at various current densities with an electrochemical window of 0~0.45 V (Fig. 5b). The presence of the triangular symmetry and linear slopes with respect to the charging/discharging curves confirm again a good electrochemical performance. The specific capacitance of the NiO nanosheet arrays obtained from the discharging curves is calculated to be 674.2 F g⁻¹ at the current density of 1 A g⁻¹, which is higher than the previous NiO electrodes,^{28, 29, 37-40} indicating that the highly porous structure and the high specific surface area of the NiO nanosheet arrays facilitate ion transfer to the porous structure. The rate capability is another important factor required for practical applications. We further investigate the relationship between the specific capacitances and current densities of NiO electrode (Fig. 5c), and find that the specific capacitance decreases with the increase of the current density. The decrease in specific capacitance at high current densities is due to an increase of the internal diffusion resistance within the pseudoactive material, which decreases the efficiency of utilization of the active material. The mesoporous NiO nanosheet arrays electrode retains 64.3% of its initial capacitance when the current density increases from 1 to 20 A g⁻¹, revealing its good rate property. The excellent rate capability is mainly attributed to the following merits. First, the mesoporous NiO nanosheets provide a large specific surface area for

electrolyte access and shorten the diffusion path in solid phase, resulting in fast redox reactions. On the other hand, the NiO nanosheets grow directly on Ni foam substrate without any non-electroactive binder, which can enhance the conductivity as well as the electrochemical performance of the electrode.

Additionally, the impedances of the NiO electrode was measured in the frequency range from 100 kHz to 0.01 Hz at the open circuit potential by applying an AC voltage with 5 mV amplitude (Fig. 5d). The Nyquist plot shows a semicircle at the high-frequency, followed by a linear part at the low-frequency region. The EIS data can be fitted by the internal resistance (R_s), the double layer capacitor (C_{dl}), the charge transfer resistance (R_{ct}), the Warburg impedance (Z_w), and the C_L for the limited pseudo-faradic reaction, as shown in the inset in Fig. 5d. Based on the equivalent electrical circuit model, the charge transfer resistances of the NiO nanosheet arrays electrode was estimated as 0.66 Ω . The small charge transfer resistance of the mesoporous NiO nanosheet arrays was attributed to the direct and close contact of the Ni foam substrate, indicating the high electronic conductivity. In addition, the nearly straight vertical line indicates a low diffusion resistance and shows good capacitor behavior of the mesoporous NiO nanosheet arrays electrode.

The long-term cycle stability represents a significant parameter for the practical applications of supercapacitors. Fig. 6 depicts the cycling stability of the as-prepared mesoporous NiO nanosheet arrays on Ni foam by conducting charging/discharging tests at a current density of 10 A g⁻¹ for 5000 cycles. It is found that the specific capacitance of the NiO electrode gradually increased during initial cycling tests, and then tended towards a slight degradation in the final cycling test. The increase of the specific capacitance is ascribed to an activation process occurring at the beginning of the charging/discharging cycling test. During this process, with the electrolyte gradually penetrating into the electrode, more and more electrode materials become activated, thus contributing to the increase of

the specific capacitance.^{41,42} Furthermore, the capacitance increase of the NiO nanosheet arrays may be attributed to the activation process that allows the trapped ions (ions can be trapped between the NiO crystalline layers during the growth of nanosheets) to gradually diffuse out.⁴³⁻⁴⁵ After 5000 cycles, the specific capacitance of the NiO electrode maintains 93.5% of its initial value, indicating the excellent cycling stability of the mesoporous NiO nanosheet arrays. The capacitance loss may be due to the loss of the electrical contact between the active materials (NiO nanosheets) and Ni foam because of change in volume of the active materials during cycling. The charge-discharge curve of the last 10 cycles of the electrode was shown in the inset of Fig. 6. The charge curves are still symmetric as compared to their corresponding discharge counterparts, indicating no significant structural change for the NiO electrode during the charge-discharge processes, as further confirmed by the SEM image of the mesoporous NiO nanosheet arrays after 5000 electrochemical cycles (see ESI, Fig. S6). The charging/discharging curves and CV curves after 1st and 5000th cycles (see ESI, Fig. S7) also verify the excellent cycling stability of the mesoporous NiO nanosheet arrays electrode, which is consistent with the EIS results of the NiO electrode during charging/discharging cycles (see ESI, Fig. S8). These results highlight the capability of the mesoporous NiO nanosheet arrays electrode to meet the requirements of both high specific capacitance and excellent cycling stability, which are important merits for the high-performance supercapacitors.

4. Conclusions

In summary, we have developed a facile and cost-effective strategy to fabricate single-crystalline NiO nanosheet arrays on Ni foam with high electrochemical performance for supercapacitors. The as-prepared mesoporous NiO nanosheet arrays electrode delivers high capacitance (674.2 F g^{-1} at a current density of 1 A g^{-1}), desirable rate capability, and excellent cycling stability (93.5% capacitance

retention after 5000 cycles). Such intriguing capacitive behavior is attributed to the unique mesoporous microstructure of the single-crystalline NiO nanosheet arrays and the smart design of the binder-free electrode. These results suggest that the binder-free mesoporous NiO nanosheet arrays electrode could be a promising candidate for high-performance supercapacitors and the cost-effective electrode design strategy can be generalized to other transition metal oxides with unique arrays structures on conducting substrates for large scale supercapacitor applications.

Acknowledgment

The authors gratefully acknowledge the financial supports provided by National Natural Science Foundation of China (Grant no. 51104194), Doctoral Fund of Ministry of Education of China (20110191120014), No. 43 Scientific Research Foundation for the Returned Overseas Chinese Scholars, National Key laboratory of Fundamental Science of Micro/Nano-device and System Technology (2013MS06, Chongqing University), State Education Ministry and Fundamental Research Funds for the Central Universities (Project no. CDJZR12248801, CDJZR12135501, and CDJZR13130035, Chongqing University, PR China).

Notes and references

^a College of Material Science and Engineering, Chongqing University, Chongqing, 400044, China. TEL.:+86 23 65104131; E-mail: zhangyuxin@cqu.edu.cn

^b College of Chemical Engineering, Sichuan University, Chengdu, Sichuan, 610065, China. E-mail: junyiji@scu.edu.cn

^c Key Laboratory of Fundamental Science of Micro/Nano-Devices and System Technology, Chongqing University, Chongqing, 400044, China

† Electronic supplementary information (ESI) available.

1 J. R. Miller and P. Simon, *Science*, 2008, **321**, 651-652.

2 P. Simon and Y. Gogotsi, *Nat. Mater.*, 2008, **7**, 845-854.

3 C. Liu, F. Li, L.-P. Ma and H.-M. Cheng, *Adv. Mater.*, 2010, **22**, E28-E62.

4 J. Tian, Z. Xing, Q. Chu, Q. Liu, A. M. Asiri, A. H. Qusti, A. O. Al-Youbi and X. Sun,

- CrystEngComm*, 2013, **15**, 8300-8305.
- 5 L. L. Zhang and X. S. Zhao, *Chem. Soc. Rev.*, 2009, **38**, 2520-2531.
- 6 G. Wang, L. Zhang and J. Zhang, *Chem. Soc. Rev.*, 2012, **41**, 797-828.
- 7 W. Wei, X. Cui, W. Chen and D. G. Ivey, *Chem. Soc. Rev.*, 2011, **40**, 1697-1721.
- 8 W. Zhou, X. Cao, Z. Zeng, W. Shi, Y. Zhu, Q. Yan, H. Liu, J. Wang and H. Zhang, *Energy Environ. Sci.*, 2013, **6**, 2216-2221.
- 9 P. Yang, X. Xiao, Y. Li, Y. Ding, P. Qiang, X. Tan, W. Mai, Z. Lin, W. Wu, T. Li, H. Jin, P. Liu, J. Zhou, C. P. Wong and Z. L. Wang, *ACS Nano*, 2013, **7**, 2617-2626.
- 10 Y. Liu, D. Yan, R. Zhuo, S. Li, Z. Wu, J. Wang, P. Ren, P. Yan and Z. Geng, *J. Power Sources*, 2013, **242**, 78-85.
- 11 Y. Zhang, C. Sun, P. Lu, K. Li, S. Song and D. Xue, *CrystEngComm*, 2012, **14**, 5892-5897.
- 12 P. Lu, F. Liu, D. Xue, H. Yang and Y. Liu, *Electrochim. Acta*, 2012, **78**, 1-10.
- 13 M.-G. Jeong, K. Zhuo, S. Cherevko, W.-J. Kim and C.-H. Chung, *J. Power Sources*, 2013, **244**, 806-811.
- 14 X. Wu, Y. Zeng, H. Gao, J. Su, J. Liu and Z. Zhu, *J. Mater. Chem. A*, 2013, **1**, 469-472.
- 15 X.-H. Xia, J.-P. Tu, X.-L. Wang, C.-D. Gu and X.-B. Zhao, *Chem. Commun.*, 2011, **47**, 5786-5788.
- 16 X. Zhang, W. Shi, J. Zhu, W. Zhao, J. Ma, S. Mhaisalkar, T. L. Maria, Y. Yang, H. Zhang, H. H. Hng and Q. Yan, *Nano Res.*, 2010, **3**, 643-652.
- 17 Y. X. Zhang, M. Huang, F. Li, X. L. Wang and Z. Q. Wen, *J. Power Sources*, 2014, **246**, 449-456.
- 18 Y. X. Zhang, M. Huang, F. Li and Z. Q. Wen, *Int. J. Electrochem. Sci.*, 2013, **8**, 8645-8661.
- 19 Q. T. Qu, L. L. Liu, Y. P. Wu and R. Holze, *Electrochim. Acta*, 2013, **96**, 8-12.
- 20 A. K. Mondal, D. Su, Y. Wang, S. Chen, Q. Liu and G. Wang, *J. Alloys Compd.*, 2013, **582**, 522-527.
- 21 S.-I. Kim, J.-S. Lee, H.-J. Ahn, H.-K. Song and J.-H. Jang, *ACS Appl. Mater. Interfaces*, 2013, **5**, 1596-1603.
- 22 S. Vijayakumar, S. Nagamuthu and G. Muralidharan, *ACS Appl. Mater. Interfaces*, 2013, **5**, 2188-2196.
- 23 J.-H. Kim, K. Zhu, Y. Yan, C. L. Perkins and A. J. Frank, *Nano Lett.*, 2010, **10**, 4099-4104.
- 24 B. Wang, J. S. Chen, Z. Wang, S. Madhavi and X. W. Lou, *Adv. Energy Mater.*, 2012, **2**, 1188-1192.
- 25 J. Li, W. Zhao, F. Huang, A. Manivannan and N. Wu, *Nanoscale*, 2011, **3**, 5103-5109.
- 26 C. Yuan, J. Li, L. Hou, L. Yang, L. Shen and X. Zhang, *Electrochim. Acta*, 2012, **78**, 532-538.
- 27 Z. Lu, Z. Chang, J. Liu and X. Sun, *Nano Res.*, 2011, **4**, 658-665.
- 28 J. Zhu, J. Jiang, J. Liu, R. Ding, H. Ding, Y. Feng, G. Wei and X. Huang, *J. Solid State Chem.*, 2011, **184**, 578-583.
- 29 Y. Q. Zhang, X. H. Xia, J. P. Tu, Y. J. Mai, S. J. Shi, X. L. Wang and C. D. Gu, *J. Power Sources*, 2012, **199**, 413-417.
- 30 F. Cao, G. X. Pan, P. S. Tang and H. F. Chen, *Mater. Res. Bull.*, 2013, **48**, 1178-1183.
- 31 M.-S. Wu, C.-H. Yang and M.-J. Wang, *Electrochim. Acta*, 2008, **54**, 155-161.
- 32 X. H. Huang, J. P. Tu, X. H. Xia, X. L. Wang, J. Y. Xiang, L. Zhang and Y. Zhou, *J. Power Sources*, 2009, **188**, 588-591.
- 33 K. Matsui, T. Kyotani and A. Tomita, *Adv. Mater.*, 2002, **14**, 1216-1219.
- 34 J. Zhong, X. L. Wang, X. H. Xia, C. D. Gu, J. Y. Xiang, J. Zhang and J. P. Tu, *J. Alloys Compd.*, 2011, **509**, 3889-3893.
- 35 J. Hu, K. Zhu, L. Chen, H. Yang, Z. Li, A. Suchopar and R. Richards, *Adv. Mater.*, 2008, **20**, 267-271.

- 36 D.-B. Kuang, B.-X. Lei, Y.-P. Pan, X.-Y. Yu and C.-Y. Su, *J. Phys. Chem. C*, 2009, **113**, 5508-5513.
- 37 D. Han, P. Xu, X. Jing, J. Wang, P. Yang, Q. Shen, J. Liu, D. Song, Z. Gao and M. Zhang, *J. Power Sources*, 2013, **235**, 45-53.
- 38 X. Li, S. Xiong, J. Li, J. Bai and Y. Qian, *J. Mater. Chem.*, 2012, **22**, 14276-14283.
- 39 X.-H. Xia, J.-P. Tu, X.-L. Wang, C.-D. Gu and X.-B. Zhao, *J. Mater. Chem.*, 2011, **21**, 671-679.
- 40 C.-Y. Cao, W. Guo, Z.-M. Cui, W.-G. Song and W. Cai, *J. Mater. Chem.*, 2011, **21**, 3204-3209.
- 41 X. Xia, J. Tu, Y. Zhang, X. Wang, C. Gu, X.-b. Zhao and H. J. Fan, *ACS Nano*, 2012, **6**, 5531-5538.
- 42 W. Li, G. Li, J. Sun, R. Zou, K. Xu, Y. Sun, Z. Chen, J. Yang and J. Hu, *Nanoscale*, 2013, **5**, 2901-2908.
- 43 J. Ji, L. L. Zhang, H. Ji, Y. Li, X. Zhao, X. Bai, X. Fan, F. Zhang and R. S. Ruoff, *ACS Nano*, 2013, **7**, 6237-6243.
- 44 X. Cao, Y. Shi, W. Shi, G. Lu, X. Huang, Q. Yan, Q. Zhang and H. Zhang, *Small*, 2011, **7**, 3163-3168.
- 45 C. Yuan, X. Zhang, L. Su, B. Gao and L. Shen, *J. Mater. Chem.*, 2009, **19**, 5772-5777.

Figures captions

Fig. 1. XRD pattern of the as-prepared NiO nanosheets arrays on Ni foam.

Fig. 2. SEM images of the Ni foam (a), NiO nanosheets on Ni foam (b-d) with different magnifications.

The insets show the corresponding optical images of the Ni foam, and NiO nanosheets on Ni foam.

Fig. 3. (a, b) Low-magnification TEM images of the mesoporous NiO nanosheet. Bottom-right inset in (b) is the corresponding SAED pattern. (c) HRTEM image of the edge part of the NiO nanosheet.

Fig. 4. Nitrogen adsorption-desorption isotherms (a) and the pore size distribution plot from the adsorption branch (b) of the NiO nanosheets.

Fig. 5. (a) Cyclic voltammograms of NiO nanosheet arrays electrode in 1 M KOH aqueous electrolyte; (b) charge-discharge curves at different current densities; (c) specific capacitance measured at different current densities; (d) the electrochemical impedance spectra of the porous NiO nanosheets electrode in the frequency range from 0.01 Hz to 100 kHz. The inset shows the enlarged EIS spectra and the equivalent circuit.

Fig. 6. Cycling performance of the electrode measured at the current density of 10 A g⁻¹. The inset shows the charge-discharge curves of the last 10 cycles of the NiO electrode.

Fig. 1.

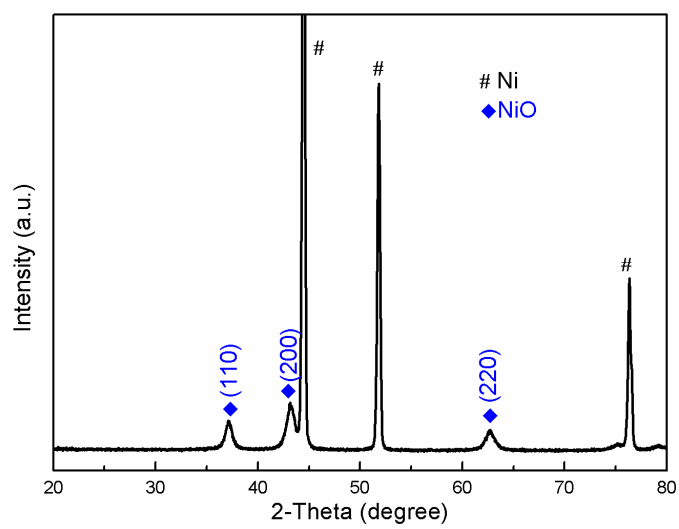


Fig. 2.

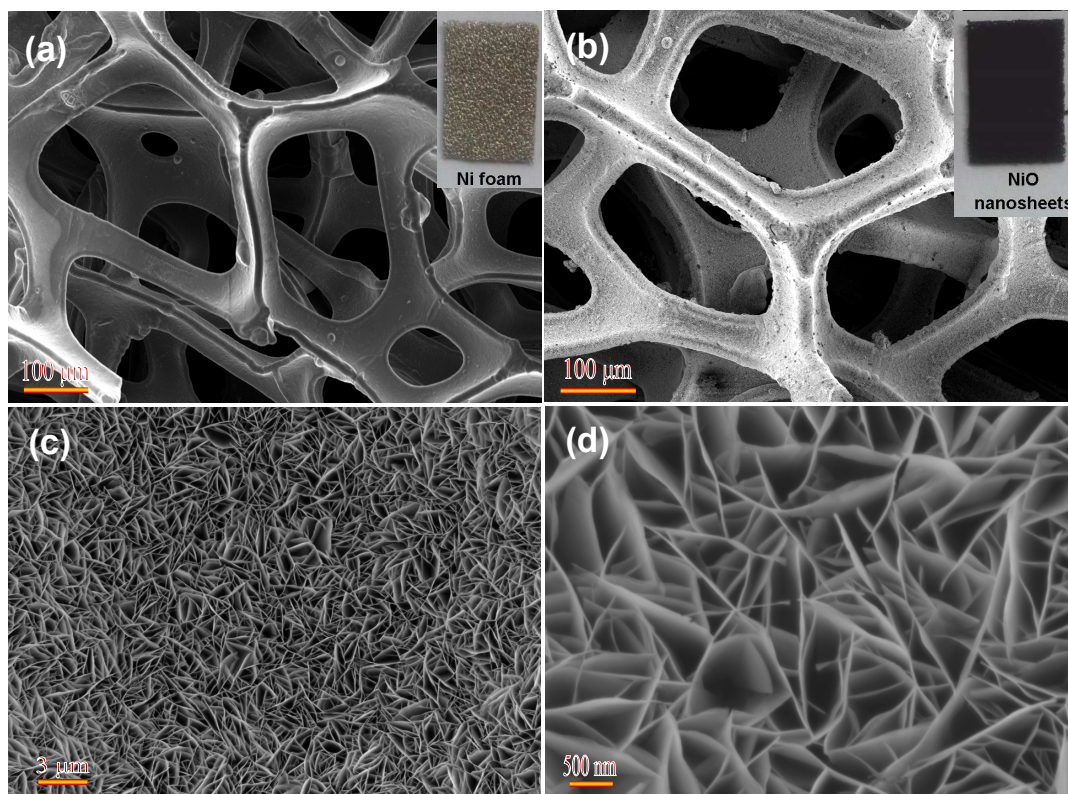


Fig. 3.

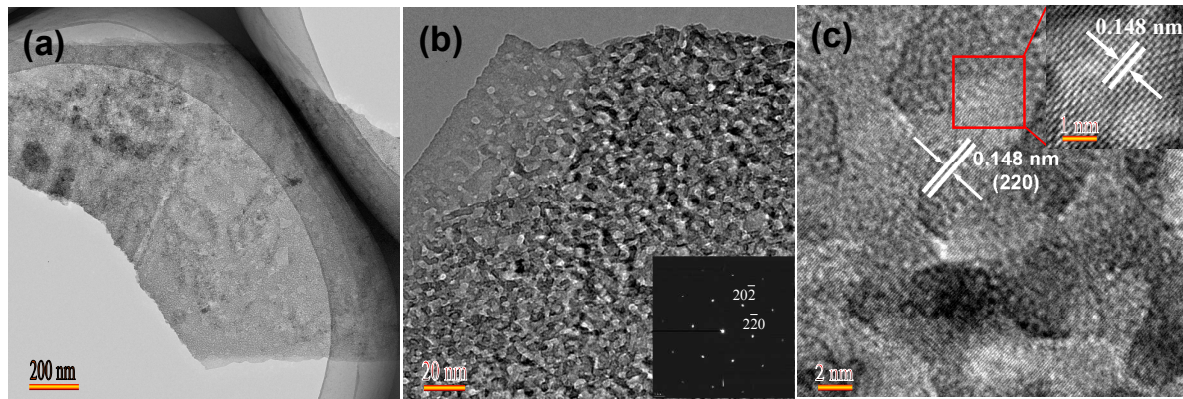


Fig. 4.

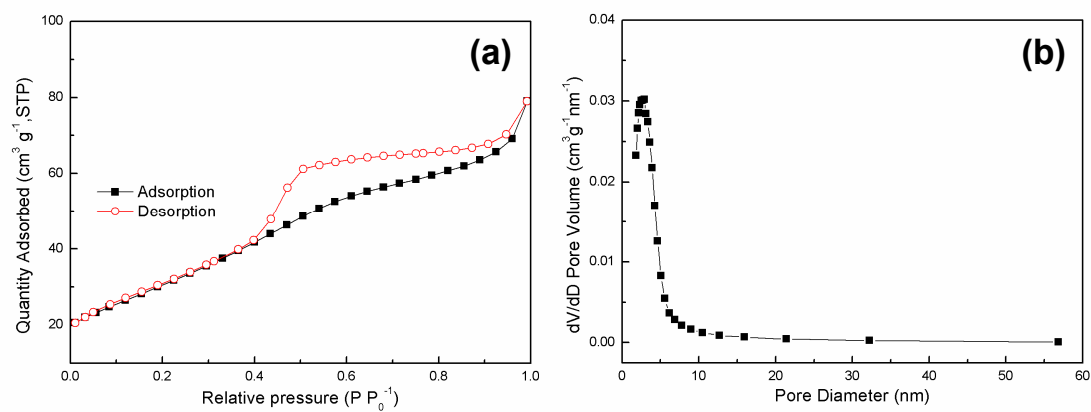


Fig. 5.

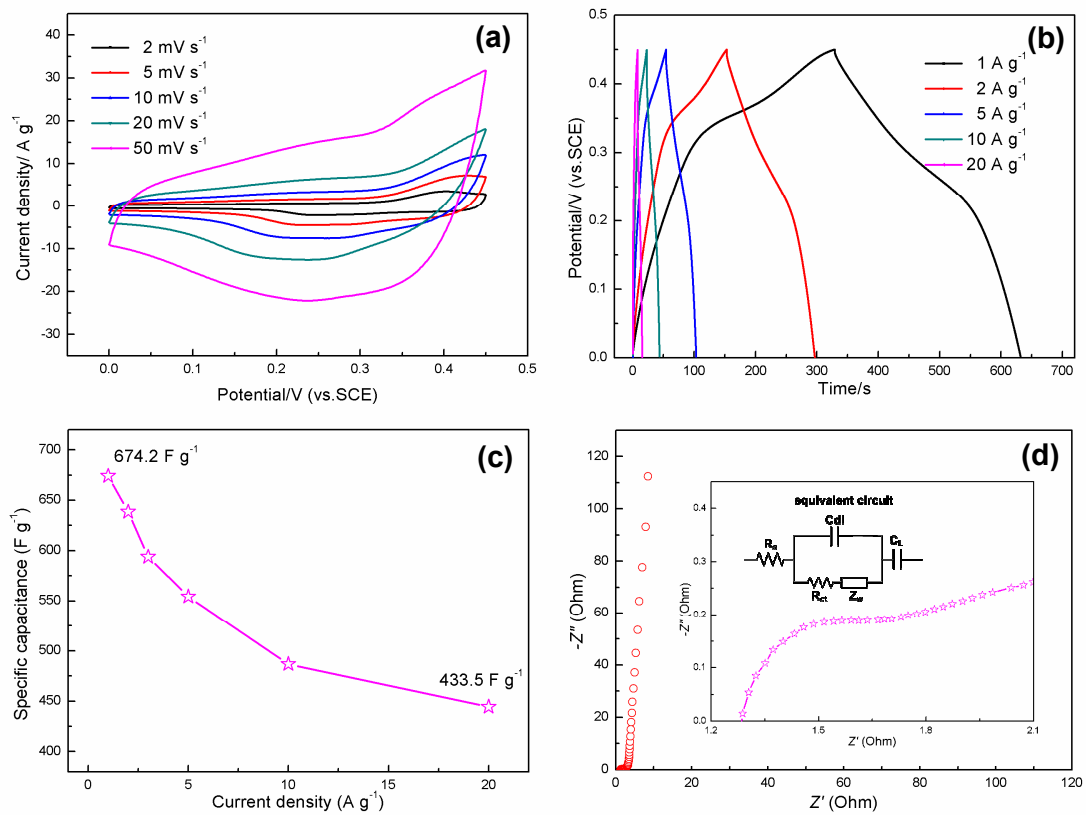


Fig. 6.

